Journal of Power Sources 273 (2015) 863–872

Contents lists available at ScienceDirect

Journal of Power Sources

journal homepage: www.elsevier.com/locate/jpowsour

Plasma properties during magnetron sputtering of lithium phosphorous oxynitride thin films

Ane S. Christiansen, Eugen Stamate*, Karl Thydén, Reza Younesi, Peter Holtappels

Department of Energy Conversion and Storage, Technical University of Denmark, Frederiksborgvej 399, 4000 Roskilde, Denmark

HIGHLIGHTS

- LiPON thin films were investigated by FIB-SEM.
- Plasma parameters were measured by mass spectrometry, probes and emission spectroscopy.
- Best film conductivity is correlated with a higher degree of dissociation for N_2.
- Higher ion energy and larger fractions of Li, P and NP are also important.

ARTICLE INFO

Article history:
Received 23 June 2014
Received in revised form
17 September 2014
Accepted 26 September 2014
Available online 5 October 2014

Keywords:
Lipon
Lithium batteries
Magnetron sputtering
Thin films
Plasma diagnostics

ABSTRACT

The nitrogen dissociation and plasma parameters during radio frequency sputtering of lithium phosphorus oxynitride thin films in nitrogen gas are investigated by mass appearance spectrometry, electrostatic probes and optical emission spectroscopy, and the results are correlated with electrochemical properties and microstructure of the films. Low pressure and moderate power are associated with lower plasma density, higher electron temperature, higher plasma potential and larger diffusion length for sputtered particles. This combination of parameters favors the presence of more atomic nitrogen, a fact that correlates with a higher ionic conductivity. Despite of lower plasma density the film grows faster at lower pressure where the higher plasma potential, translated into higher energy for impinging ions on the substrate, resulted in a compact and smooth film structure. Higher pressures showed much less nitrogen dissociation and lower ion energy with thinner films, less ionic conductivity and poor film structure with large roughness.

1. Introduction

The increasing demand on portable microelectronic devices (sensors, circuit boards, etc.) has made the development of compact, all-solid-state thin film batteries a field of increasing importance. A common requirement for the batteries is that they need to be compact, of low weight and of high power density. Thus, improving the performance, i.e. capacity, lifetime and safety, and lowering the cost of batteries is a critical goal under stringent need for development. Lithium ion based batteries are often chosen due to their high power density and low weight. The main active components in a battery are the cathode, anode and electrolyte. The requirements for a good solid electrolyte includes a high ionic conductivity, low electronic conductivity, electrochemical stability in a wide potential range, good performance in a wide temperature range, homogeneous morphology without pores or cracks, and good adhesion with the electrode materials. Lithium phosphorous oxynitride (Lipon) [1,2] thin films is one of the most promising electrolyte materials for compact solid-state-battery [3–6]. It was initially developed in the 1990's by Oak Ridge National Laboratories and is an amorphous Li^+ ion conductor with a very high electrochemical stability window of between 0 V and 5.5 V vs. Li/Li^+ [7], which makes it compatible with high-voltage cathodes, as well as stable in contact with lithium metal [1]. In addition it shows an acceptable Li ion conductivity ($\sigma_{Li+} \approx 2 \cdot 10^{-6}$ S cm^{-1}) [7] and low electron conductivity ($\sigma_{e-} = 8 \cdot 10^{-14}$ S cm^{-1}) [8] at 25 °C depending on the exact stoichiometry, usually close to $Li_{3.3}PO_{3.9}N_{0.17}$ [1]. Due to the amorphous structure Lipon has the advantages of isotropic conduction properties and in addition it can form flexible thin films [9] and exerts no cracking even when cathode volume changes [7]. This makes it very interesting for commercial applications. Besides being used as solid electrolyte, Lipon is also interesting as a particle coating to stabilize high voltage cathodes [10–13].

* Corresponding author. Tel.: +45 4677 4562; fax: +45 4677 4565.
E-mail address: eust@dtu.dk (E. Stamate).

http://dx.doi.org/10.1016/j.jpowsour.2014.09.174
0378-7753/

Several deposition techniques have been used to produce Lipon thin films, including: radio frequency (RF) magnetron sputtering [4,14–19], pulsed laser deposition [20], electron beam evaporation [21], ammonolysis [22], plasma assisted vapor deposition [23], and ion beam directed assembly [24]. Reactive magnetron sputtering is the technique most often used, where the Lipon thin films can be formed by sputtering from a Li_3PO_4 target in pure nitrogen gas. Many parameters of the sputtering process affect the quality of the Lipon films in terms of Li ion conductivity, film morphology, and film deposition rate. This includes RF sputtering power [14–16,19,25], nitrogen pressure [16,17,19], nitrogen flow rate [25,26], substrate temperature [27], post–thermal treatment [28,29], target morphology [18,19,25], and target-to-substrate distance [19]. During the sputtering the nitrogen atoms are incorporated into the Li_3PO_4 structure by breaking the P–O–P bond and forming P–N=P and P–N$<^{P}_{P}$ bonds [30]. The introduction of triple bonded nitrogen induces a structural disorder which affects the ionic conductivity of the film considerably, however, despite extensive research this dependence is not yet well understood [31]. A new approach to better understand how the sputtering parameters affects the Lipon properties is to determine the type of reactive species formed in the plasma during the reactive sputtering. Identification of the type and concentration of reactive species in correlation with main plasma parameters (plasma density, n_e, electron temperature, T_e, and plasma potential, V_{pl}) during the Lipon sputtering could thus contribute to the understanding of the film growth mechanism and then link it to the electrochemical properties. To our knowledge such kind of plasma diagnostics during sputtering of Lipon has never been reported.

The objective of this work is to investigate the plasma properties during the reactive RF magnetron sputtering of a Li_3PO_4 target in nitrogen atmosphere using mass spectrometry, electrostatic probes and optical emission spectroscopy. The detailed plasma diagnostic is performed in an electron cyclotron resonance (ECR) plasma assisted RF sputtering setup. The influence of sputtering power and nitrogen pressure on the reactive species formed in the plasma is investigated in direct correlation with morphology and electrochemical properties of deposited Lipon films. A sputtering power in the range of 50–300 W and a nitrogen pressure in the range of 5–50 mTorr will be used. Focused ion beam scanning electron microscopy (FIB-SEM) is used for characterization of the microstructure and film morphology and electrochemical impedance spectroscopy (EIS) is used for determining the ionic conductivity of the films.

2. Experimental methods

2.1. RF magnetron sputtering

The synthesis of thin Lipon films was performed using an RF magnetron sputtering system of a 2 inch Li_3PO_4 target (Kurt Lesker®) in N_2 atmosphere. The Li_3PO_4 target was presputtered for an hour before each deposition in order to remove any impurities of hydrocarbons on the surface. The Lipon films were deposited onto 100 nm Au-coated silicon substrates using different values of N_2 pressure (5, 20, or 50 mTorr) and RF power (100, 200, or 300 W) in a controllable nitrogen flow of 66 sccm. A sputtering time of 7 h and a target-to-substrate distance of 60 mm were used in each case. The substrate temperature (below 200 °C) was dictated by heat formation from the plasma generation and no additional heating was applied. A 300 nm Ag coating was deposited on top of the Lipon layer. Proper masking during deposition of the Lipon and Ag layers, resulted in Au/Lipon/Ag cells of 7×7 mm^2.

2.2. Impedance spectroscopy

The resistances of the Lipon films were measured by AC electrochemical impedance spectroscopy (EIS). The EIS spectra of the prepared single layer Lipon films was measured by using the Ag/Lipon/Au sandwich structure. A setup consisting of spring loaded Au-plated pins implanted in a Plexiglas plate was used for the EIS measurements in a 2-electrode setup. One of the test probes was contacted to the Ag film (using a piece of conducting rubber in between) and the other was contacted to the Au coated substrate outside the cell. EIS measurements were conducted at room temperature using a Biologic VMP3 impedance analyzer in the frequency range from 10 mHz to 500 kHz. Two cells for each Lipon layer type were tested. The impedance data were analyzed by nonlinear least square fitting of the data to equivalent circuits using the EC lab software [32].

2.3. Thin film characterization

The microstructure of Lipon films prepared at 100 W was investigated using a Carl Zeiss 1540 XB (Carl Zeiss, Oberkochen, Germany) combined focused ion beam and scanning electron microscope (FIB-SEM). A Ga-ion source was used for the FIB. To create a cross-sectional view perpendicular to the Ag surface, a trench was created using a 10 nA ion-probe and the subsequent surface polish was performed using a 200 pA beam. For the SEM, an acceleration voltage of 1.5–5 keV was used and either a secondary electron (SE) or an in-lens SE detector was used for obtaining the micrographs. Lipon films prepared at 200 W and 300 W were investigated using a Carl Zeiss Supra 35 (Carl Zeiss, Oberkochen, Germany) with an acceleration voltage of 1.5–5 keV. Cross sections were prepared by fracturing these samples inside the glove box with aid from a diamond cutter on the back side. The samples were very shortly exposed to air (less than 1 min) during the transfer between glove box and SEM. The XPS measurements were performed on a commercial PHI 5500 spectrometer (Perkin Elmer Physical Electronics, Minneap-olis, MN), using monochromatized Al Kα radiation (1487 eV) and an electron emission angle of 45°. The dimensions of the measurement region were approximately 2×4 mm.

Energy dispersive spectroscopy (EDS) measurements were performed using the Carl Zeiss Supra 35 at an acceleration voltage of 10 kV. Data was collected using a “Bruker Nano XFlash Detector” and analyzed by the software “Bruker Esprit 1.9”.

2.4. Plasma diagnostics

Surface contamination of probes, additional electrodes and optical ports is the main problem for plasma diagnostics during deposition of thin films by magnetron sputtering. Even a few seconds of deposition are enough to contaminate the probe surface; a fact that results in erroneous measurements of the current-bias characteristic and consequently incorrect estimation of plasma parameters [33,34]. Films above only a few nm deposited on windows keeping the vacuum or on tips of optical fibers can also affect the emission lines detected by optical emission spectroscopy. In addition, such films can also influence the performance of a separation mesh placed in the front of the orifice of the mass spectrometer to eliminate the contribution of plasma ions when detecting the neutral radicals. For these reasons a different setup than the one used to deposit micrometer thick Lipon films was used for plasma diagnostics. The following precautions were taken to ensure a correct diagnostics. An independent plasma source was used in the same chamber with the magnetron sputtering cathode and the diagnostic equipment as to allow the cleaning of the probe surface and of the separation mesh by ionic bombardment in nitrogen plasma during

the off time of the RF sputtering. Each probe measurement was performed after 3 min of probe cleaning, for a recording time below 1 s during the sputtering, using a fast data acquisition system controlled by a PC. The mesh contamination was monitored by keeping below 5% the decrease of the collected current, due to contamination, during mass spectrometry measurement. Cleaning of the mesh with ionic bombardment was performed once the collected current deviated from the reference value corresponding to a clean surface. The tip of the optical fiber (vacuum tide) was inserted in a 10 mm long ceramic tube of 0.7 mm inner diameter and 1.2 mm outer diameter as to ensure certain directionality for optical measurement and prevent contamination. The setup is presented in Fig. 1 and includes the ECR plasma source consisting of a 3 × 4 matrix configuration of distributed plasma cells placed at the top of a 40 × 40 × 40 cm vacuum chamber. The ECR cells [35,36] can produce uniform plasma in a pressure range from 10 down to 0.1 mTorr. A water cooled magnetic filter, made of permanent magnets, is used to control the electron temperature [37]. The 2 inch magnetron sputtering cathode is placed on the lateral side facing the head of a Hiden mass spectrometer, with a distance of 130 mm from the entrance orifice to the cathode. The Langmuir probe and an optical fiber is inserted perpendicular to the direction of the mass spectrometer and the cathode (6.5 cm from the cathode surface in the axial direction and 2.5 cm off axis) as to measure plasma parameters and optical emission spectra. The current–voltage probe characteristics were used to obtain plasma density, n_i, from the ionic saturation region, the effective electron temperature, T_{eff}, by integrating the electron energy distribution function, and plasma potential, V_{pl}, as the potential giving the maximum value of the first derivative of the current–voltage characteristic [38,39].

It is expected that the atomic nitrogen can influence the ionic conductivity of the Lipon films. So it is important to estimate the fraction of atomic nitrogen into discharge and also to detect other ions and reactive species assisting the film growth. The ionization degree of magnetron plasmas is below 10% and the ionization efficiency of the filament placed inside of the mass spectrometer head, as to detect neutral species, is about 10^{-4}. It means that the detection of atomic nitrogen is only possible by eliminating the N^+ originated from plasma. At the same time the ionization filament can dissociate the N_2 and N_2^+ inside of the mass spectrometer, contributing indirectly to the atomic nitrogen peak. In order to avoid these problems, the nitrogen ions originating from plasma were reflected before the entrance into the mass spectrometer using a biased mesh of 15 mm diameter and placed 10 mm in front of the orifice. The mesh was biased at 10 V with respect to V_{pl} (detected by probe) when measuring radicals and was kept at V_{pl} for when measuring ions. Also, in order to discriminate between the atomic nitrogen created in plasma from that created by the ionizing filament through dissociation, we used the method of mass appearance spectroscopy proposed by Sugai et al. [40] which takes into account the threshold energy for dissociation of N_2.

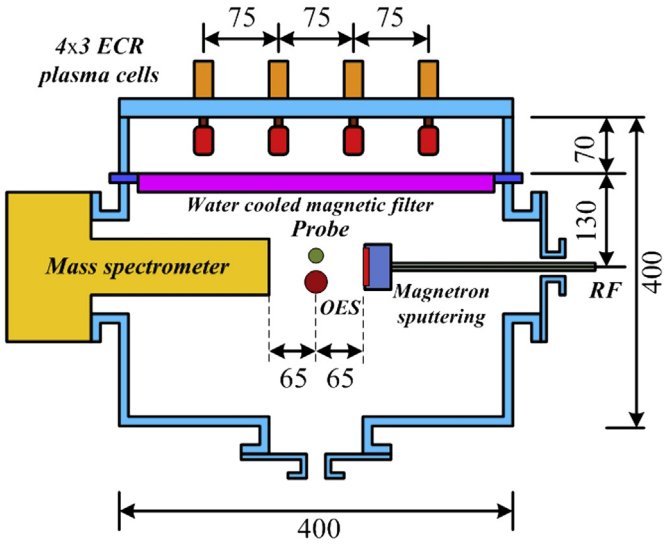

Fig. 1. Schematic of the sputtering system including the ECR plasma cells and the diagnostics equipment.

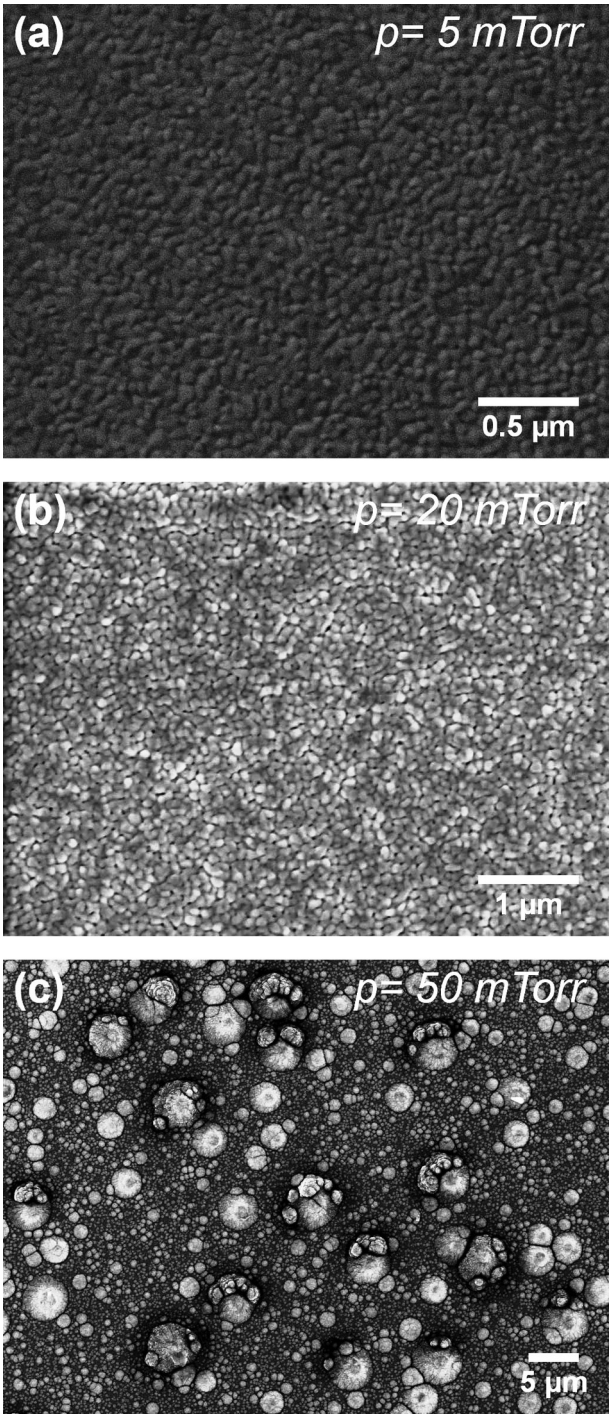

Fig. 2. SEM micrographs of the surface of Lipon films (Ag-coated) deposited with RF power of 100 W and a N_2 pressure of (a) 5 mTorr, (b) 20 mTorr, and (c) 50 mTorr.

Therefore, N was detected by applying an ionization potential of 21 V to the filament while N_2 was detected for 14 V.

3. Results and discussion

3.1. Microstructure

3.1.1. Effect of nitrogen pressure

Top view SEM of the Ag-coated Lipon films deposited in a nitrogen pressure of (a) 5 mTorr, (b) 20 mTorr and (c) 50 mTorr are presented in Fig. 2 for a RF power of 100 W and 7 h of deposition time. The magnifications are not identical as to make it easier to identify the large differences on morphology. A uniform film surface was observed for 5 and 20 mTorr, while well distinct structures of micrometer size are present for 50 mTorr. To investigate the morphology in more detail FIB-SEM micrographs of the cross section of the films are presented in Fig. 3. The films prepared at 5 mTorr and 20 mTorr are compact, uniform, and without cracks or voids. Both films have a very good contact with the Ag layer and the substrate (see Fig. 3(b) and (d)). The film prepared at 50 mTorr, on the other hand, has a very rough, irregular morphology with the presence of large volcano-shaped micro-structures at the surface. As can be seen from Fig. 3(f), the origin of these volcano-structures comes from irregular growth of the Lipon layer itself. The influence of nitrogen pressure on the Lipon morphology can be compared to the work by Chiu et al. [41] and Park et al. [17]. Both groups have found that using a nitrogen pressure at/above 20 mTorr results in a rough, irregular layer structure. This observation can be explained by the fact that at higher pressure the mean free path of the sputtered atoms are shorter due to a higher collision frequency [42]. This reduces the kinetic energy of the particles and thereby their ability for surface diffusion after deposition on the substrate [43]. The lower diffusion energy of the deposited particles will result in a rough surface structure with potential voids and pinholes. Despite similarities with other studies, the observation of volcano-shaped micro structures has never been published before. All three Lipon films were made using a sputtering time of 7 h, but large differences in the final layer thickness was observed. At 5 mTorr a thickness of 1.43 μm was obtained, corresponding to a sputtering rate of 3.4 nm min^{-1}. At 20 mTorr a thickness of 0.97 μm was obtained, while at 50 mTorr the thickness at the flat Lipon layer (excluding the volcano-structures) is only 0.59 μm. From this it is clear that the nitrogen pressure affects the deposition rate of the Lipon layers, with a low pressure giving the highest deposition rate. This trend is expected because a high sputtering pressure will increase the scattering of the sputtered atoms and thereby reduce the amount of sputtering particles that hits the substrate and thus decrease the deposition rate [42]. This trend was also observed by Hamon et al. [19].

3.1.2. Effect of RF power

SEM micrographs of Ag-coated Lipon films deposited using a nitrogen pressure of 5 mTorr and an RF power of 200 W and 300 W,

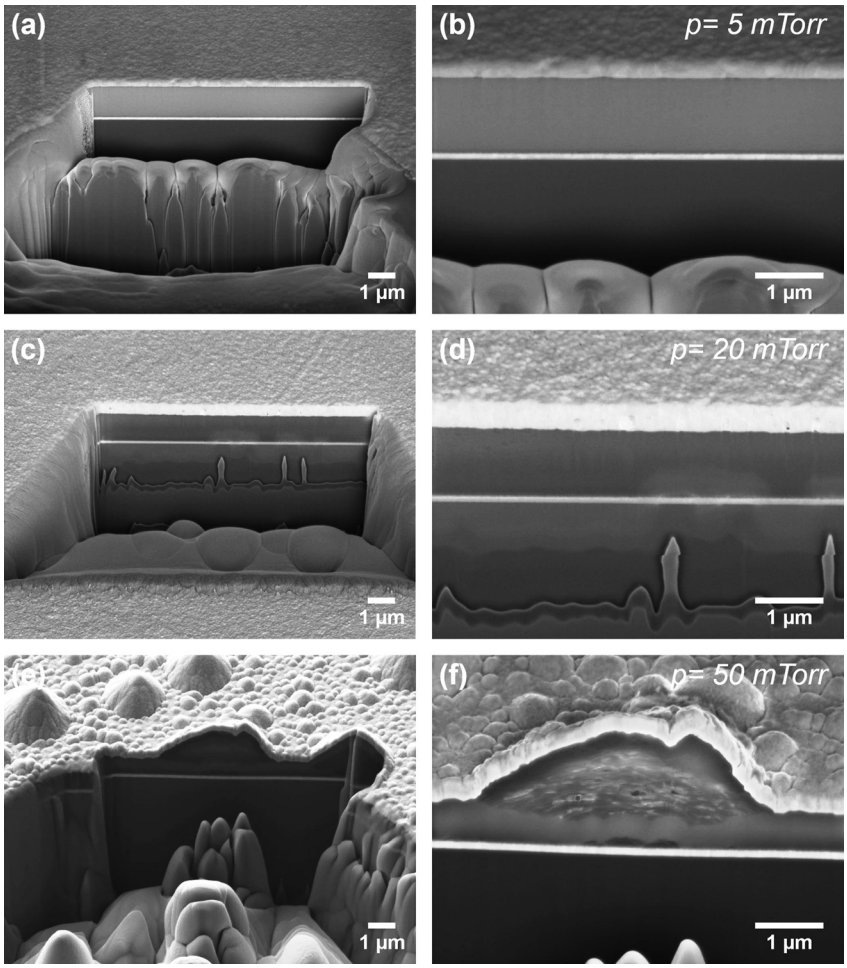

Fig. 3. FIB-SEM micrographs of Ag/Lipon/Au structures on Si substrate, with higher magnification in the right-hand-side for similar conditions as in the left. The Lipon films were deposited at 100 W at a N_2 pressure of (a) and (b) 5 mTorr, (c) and (d) 20 mTorr, and, (e) and (f) 50 mTorr, respectively.

respectively, are presented in Fig. 4. Both samples have a Lipon layer that is very coarse, causing the Ag-coating to be very rough. When comparing to the film formed using an RF power of 100 W (Fig. 3(a) and (b)) a significant difference is observed. Although the cross section of the samples in Fig. 4 are the edge of a broken sample, and not a FIB-milled smooth surface as seen in Fig. 3, the difference in Lipon layer structure is obvious. Using a sputtering power above 200 W results in a Lipon layer with a very bad contact with the Ag layer. The surface of the sample prepared at 200 W (Fig. 4(b)) has the presence of large crater-like irregularities. These craters have occurred during the Lipon deposition, as the bottom of the craters shows a layer of Ag on top of the Au substrate (i.e. local sites where Au and Ag are contacted). Due to the presence of these pinholes the samples prepared at 200 W were short-circuited, and no electrochemical characterization could be performed. The presence of craters in the Lipon film could be explained by the generation of particles from the target at high RF power [45]. Due to the top-down sputtering configuration the particles will fall onto the substrate and eventually cause pinholes in the Lipon layer. The sample prepared at 300 W (Fig. 4(c) and (d)) suffers from severe cracks, due to stress, through the Lipon layer and large regions of delaminated Ag top layer. These samples were also short-circuited. The presented results show that an RF sputtering power around 100 W gives the best films, which also agrees well with the reports by other groups [14–16,19,25]. The estimated thickness of the sample prepared at 200 W is 2.9 μm, while for the sample prepared at 300 W it is 4.6 μm (11 nm min^{-1}). Based on these values it is clear, that increasing the RF power results in increased deposition rates, as has also been observed by other groups [14–16,19], albeit with a great reduction in the Lipon layer homogeneity. The increased deposition rate is expected as a high RF power will increase the target erosion due to a larger plasma density, a fact that can also dislocate larger clusters that can land on the substrate.

3.1.3. Electron beam sensitivity

Obtaining good SEM micrographs of Lipon layers can be a challenging task as Lipon is interacting with the electron beam. Even with a low acceleration voltage of 1.5 kV, significant alterations can be observed after just a single scan. Fig. 5 shows an example of the morphological changes in a Lipon layer after multiple scans with the electron beam. After one scan in the focused area, small bulky peaks started to protrude from the smooth Lipon surface, and after a total of three scans their size had increased significantly. It is well known that oxides and other simple inorganic compounds can decompose in an electron beam [46]. The inelastic collision between the incoming electrons and the particles of the sample leads to a significant energy transfer that can generate heat as well as induce structural changes in the sample. Due to the insulating properties of Lipon the radiation damage is likely enhanced even further. Possibly local regions of crystalline phases (Li_2O, Li_3N, or Li_2CO_3) can form within the amorphous Lipon layer as a result of P–O and/or P–N bond breaking and thereby explain the observed changes. However, no exact explanation will be attempted here.

3.2. Ionic conductivity

To determine the ionic conductivity of the Lipon films electrochemical impedance spectroscopy was used. The impedance results of the samples deposited using an RF power of 100 W is presented in Fig. 6 along with the equivalent circuit used for fitting. No conductivity measurements were obtained from the samples deposited at 200 W and 300 W, as both of these samples was short-circuited due to bad film-morphology, as described earlier. The Nyquist plots consist of a depressed semicircle at the high frequency range and an almost linear segment at the low frequency range. The semicircle is ascribed to the impedance response from the Lipon film and is fitted by the parallel contribution of a resistance (R_i), which describes the ionic DC conductivity in the Lipon film, and a constant phase element (Q_i). The low frequency segment is ascribed to the electrode-Lipon interfaces. The interfaces between the Au/Ag layers and the Lipon film are neither perfectly ion-blocking nor ideally smooth. Therefore the EIS spectra do not

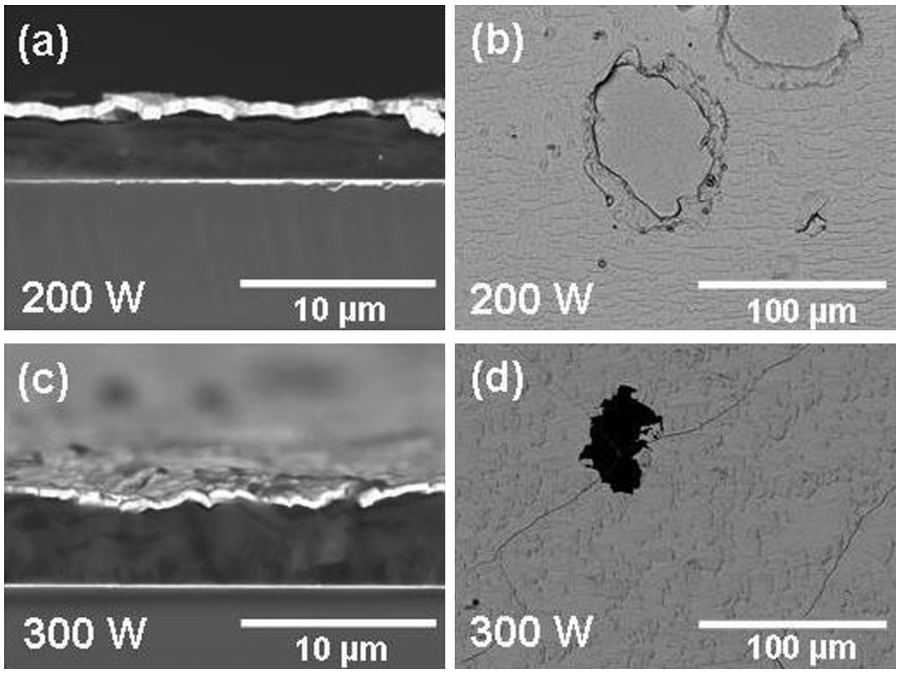

Fig. 4. SEM micrographs of Ag-coated Lipon films deposited with a nitrogen pressure of 5 mTorr and a RF power of (a) and (b) 200 W and (c) and (d) 300 W. The micrographs (a) and (c) show the cross section of a broken sample, while the ones to the right show the on-top surface structure. While (b) shows the presence of craters (d) exhibits cracks. The Lipon layer thickness was (a) 2.9 μm and (c) 4.6 μm, respectively.

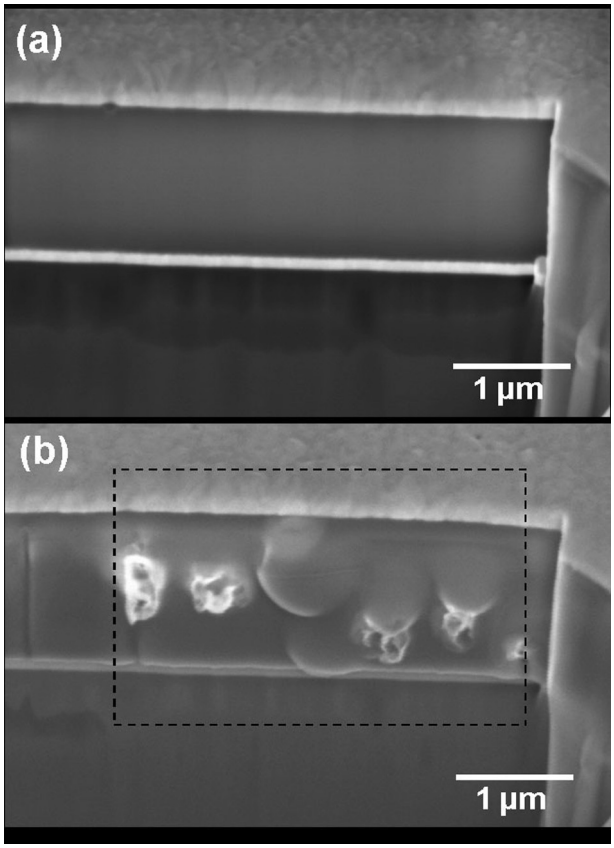

Fig. 5. FIB-SEM micrographs showing the change in morphology of a Lipon layer (100 W and 5 mTorr) after exposure to an electron beam of 1.5 kV; (a) after 1 overview scan, and (b) after 3 additional scans of the area indicated by the dashed line.

exhibit a pure capacitive response at the low frequency range as would have been expected when using ion-blocking electrodes (i.e. the curve does not meet the real axis at a 90° angle). Instead, the low frequency tail has a slope that is different from vertical. To compensate for this deviation, interfacial impedance is introduced to characterize the low frequency response, given by a second constant phase element (Q_{int}). A contact resistance (R_{ohm}) is also included in the fit, although the contribution of this to the total impedance is negligible ($R_i >> R_{ohm}$).

The ionic conductivities (σ_i) of the Lipon films are calculated based on the resistances (R_i) found from the impedance fitting and the following equation.

$$\sigma_i = \frac{d}{R_i A}, \tag{1}$$

where d is the thickness of the Lipon film and A is the area of the Ag electrode. The ionic conductivity of the Lipon layer prepared at 5 mTorr is 2.16 μS cm^{-1}, which is comparable to the maximum conductivity reported in literature so far [7]. The conductivity at 20 mTorr shows a bit lower value of 1.58 μS cm^{-1}, while the sample prepared at 50 mTorr shows the worst conductivity with only 0.47 μS cm^{-1}. The conductivity is thus highly dependent on the nitrogen pressure, where a low pressure of 5 mTorr yields a much larger conductivity than both 20 mTorr and 50 mTorr.

3.3. Plasma diagnostics

In order to understand the deposition parameters that can influence the properties of the Lipon layers, plasma diagnostics was performed using mass spectrometry, probe measurements and optical emission spectroscopy. The mass spectra for different pressures are shown in Fig. 7(a) for collected ions (grid potential set to V_{pl}) and for collected neutrals (grid potential set to V_{pl}+10 V) in

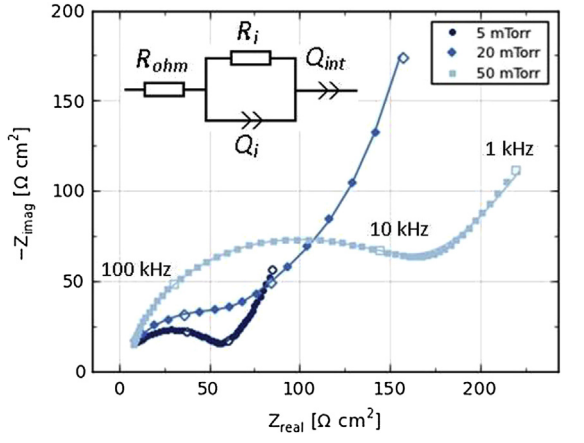

Fig. 6. Nyquist plot of the experimental impedance spectroscopy results (marks) including fit (solid line) of the Lipon films prepared at 100 W for different pressures. The open marks indicate the beginning of each new decade of frequencies. The equivalent circuit used for the fit is shown in the upper left corner.

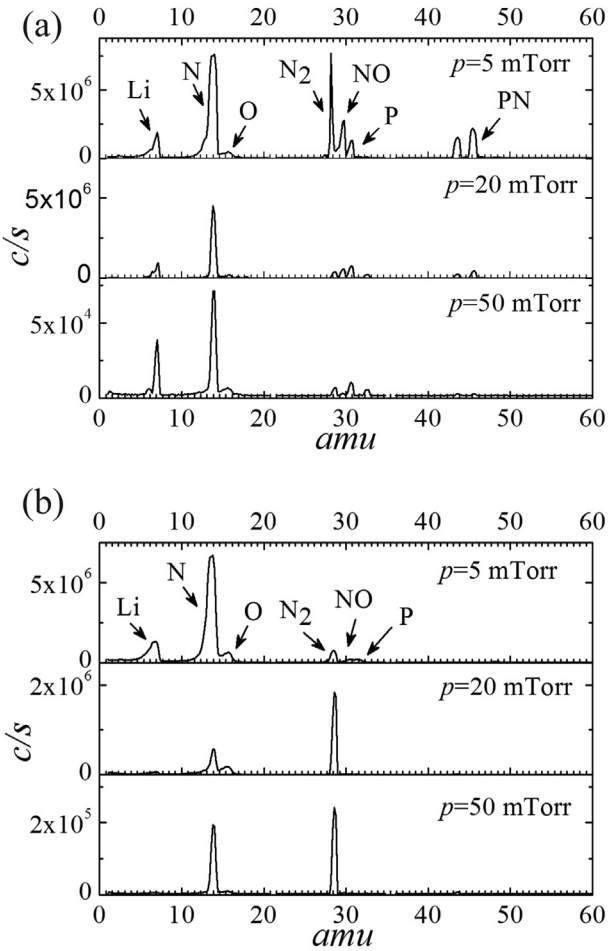

Fig. 7. Mass spectrometry measurements during the sputtering for different pressures at 100 W RF power; (a) ion species and (b) neutrals.

Fig. 7(b), respectively. A large peak of N^+ is present for all pressures in Fig. 7(a), however, it takes into account not only the ions originated from plasma but also those resulted via the dissociation induced by the ionization filament in the head of the mass spectrometer. Notable is the presence of Li, P, and small amounts of PN(45 amu), NO(30 amu) and O. Most of these species are also detected as neutrals (Fig. 7(b)). However, due to the appropriate settings of the grid potential and also the filament ionization energy, it is evident that the atomic nitrogen is present in a higher concentration than N_2 only for $p = 5$ mTorr. The peak intensity ratio of atomic N to N_2 by mass appearance spectrometry [40], as a function of RF power (P_{RF}) for different nitrogen pressures (p), is presented in Fig. 8(a). This result shows that the N_2 dissociation is significantly higher at low pressures ($p < 10$ mTorr); a fact that promotes the incorporation of nitrogen into the Lipon film structure. The peak intensity ratio of N to Li is presented in Fig. 8(b). This shows that Li is also most available at low pressures; a fact that is beneficial for a higher ionic conductivity. The intensity lines of Li^+ and P^+ ions as a function of P_{RF} for different pressures are presented in Fig. 9(a) and (b), respectively, where higher powers show larger amounts of Li^+ and P^+ while higher pressure led to lower values, due to plasma localization closer to the sputtered target, as the mean free path of ion and radical species decreases. Probe measurements of n_i as a function of RF power at different pressures are presented in Fig. 10 and reveal that the plasma density increases with RF power and also with nitrogen pressure in a range from 5×10^{15} m^{-3} up to 3×10^{16} m^{-3}. Fig. 11 shows T_{eff} and V_{pl} as a function of RF power for different pressures. The effective electron temperature was below 1.5 eV except for $p = 5$ mTorr and $P_{RF} > 150$ W, and reached more than 2 eV only at 300 W and 5 mTorr. The plasma potential was 9 V at 5 mTorr and decreased to 4 V for $p = 50$ mTorr. The optical emission spectra is presented in Fig. 12 for operation in ECR plasma in black (500 W, 5 mTorr) and magnetron sputtering discharge in red (300 W, 5 mTorr) where from one can see that two Li lines can be easily identified at 610.4 and 670.7 nm only with the sputtering on. The intensity of Li lines

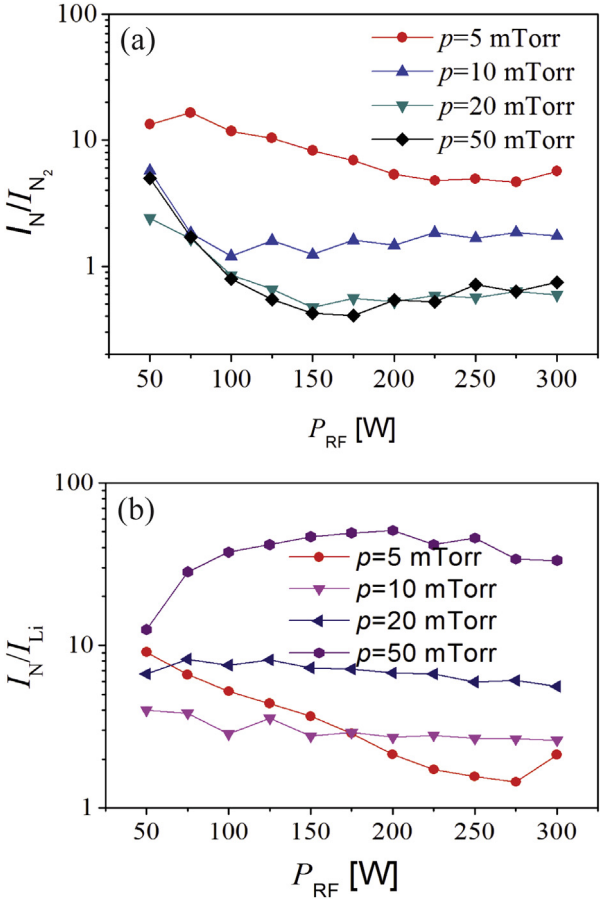

Fig. 8. Mass peak intensity ratio of (a) N to N_2 and (b) N to Li as a function of RF power for different pressures.

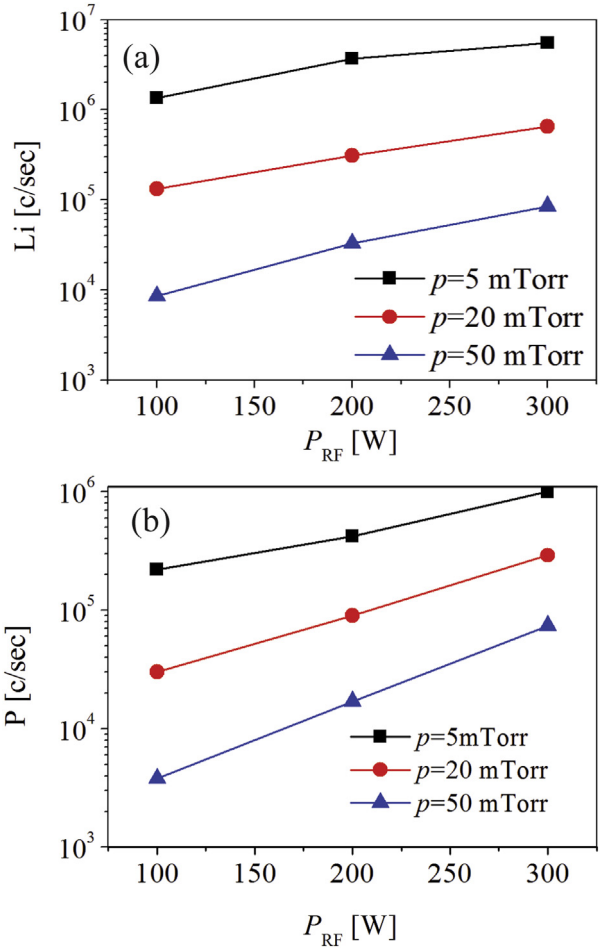

Fig. 9. Mass peak intensity of (a) Li and (b) P as a function of RF power for different pressures.

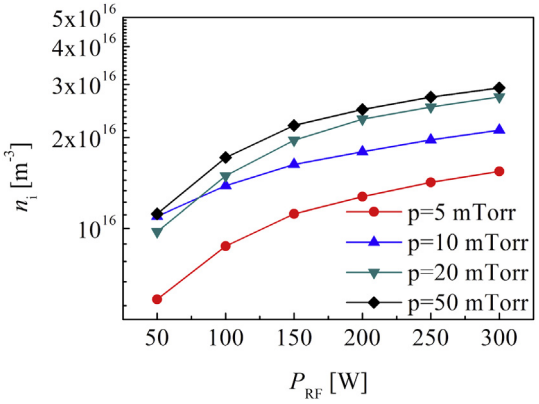

Fig. 10. Plasma density (n_i) as a function of RF power for different pressures.

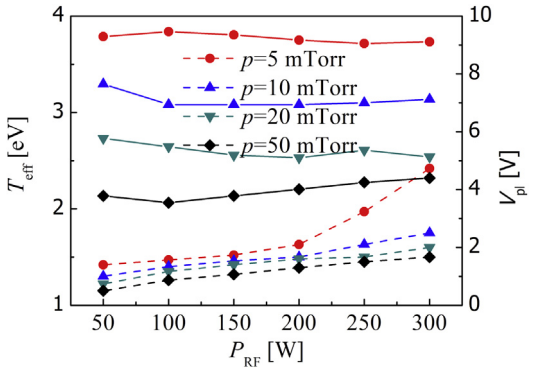

Fig. 11. Effective electron temperature (T_{eff}) with dashed lines and plasma potential (V_{pl}) with continuous lines as a function of RF power for different pressures.

as a function of discharge power for different pressures is presented in Fig. 13 and shows the same trend of increasing values with power as obtained from mass spectrometry. The pressure dependence shows higher intensity lines as the plasma gets brighter at higher pressures due to localization near the Lipon target.

Plasma parameters presented in this section show a higher degree of nitrogen dissociation at low pressure (below 10 mTorr) and moderate discharge power (below 150 W). This range of pressure is in fact close to the lowest pressure limit, of a few mTorr, able to sustain the RF magnetron sputtering discharge. More atomic nitrogen and also Li, correlated with higher ion energies, and formation of NP bonds in the gas phase, are very well correlated with thin films with higher ionic conductivity, higher deposition rate and smoother and more compact structure. N_2 is an important reactive gas used to grow various films and its dissociation has been intensively studied with results confirming the same behavior as in the present study, where higher electron temperature and lower plasma density are most favorable for producing atomic nitrogen. Probe measurements have shown clearly that less dense plasma at 5 mTorr resulted in a thicker film, grown in the presence of more energetic ions, a fact that usually results in denser films. These results are opening a possible route to investigate the yet not understood, ionic conduction mechanism, in direct correlation with the atomic nitrogen concentration in the gas phase. At the same time, even lower pressures than 5 mTorr and energetic ion assistance are promising routes to further increase the ionic conductivity of Lipon thin films.

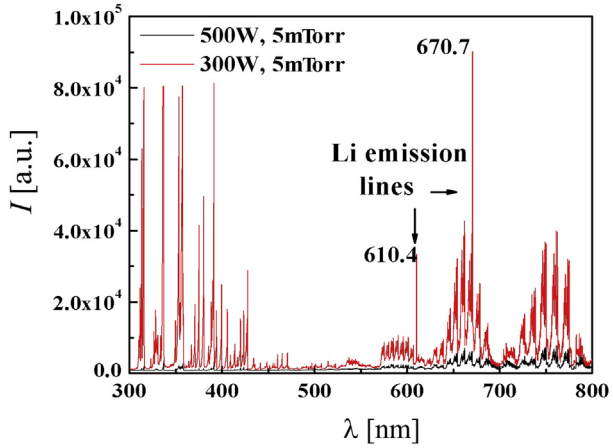

Fig. 12. Optical emission spectra for operation in ECR plasma (500 W and 5 mTorr) in black and magnetron discharge (300 W and 5 mTorr) in red. Two distinctive Li lines can be easily identified at 610.4 and 670.7 nm. (For interpretation of the references to colour in this figure legend, the reader is referred to the web version of this article.)

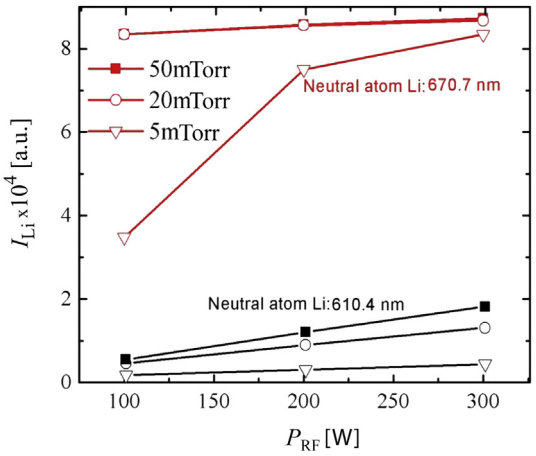

Fig. 13. The intensity of Li lines as a function of discharge power for different pressures.

3.4. Lipon film composition

To correlate the amount of atomic nitrogen in gas phase with film properties the film composition was investigated by XPS and EDS. Fig. 14 presents the (a) N1s and (b) P2p peaks by XPS for 5 and 50 mTorr, respectively, deposited for 100 W and 150 min deposition time (about 300 nm in film thickness deposited on 0.5 mm thick silicon substrate). The measurement area in about 2×4 mm^2 so the signal integrates over surface morphology structures presented in Fig. 2. Despite of higher N_2 pressure the N1s peak is higher at 5 mTorr than at 50 mTorr. A reversed trend is observed for P2p with larger content of P for 50 mTorr. The deconvolution of experimental peaks reveals comparable fractions of double and triple

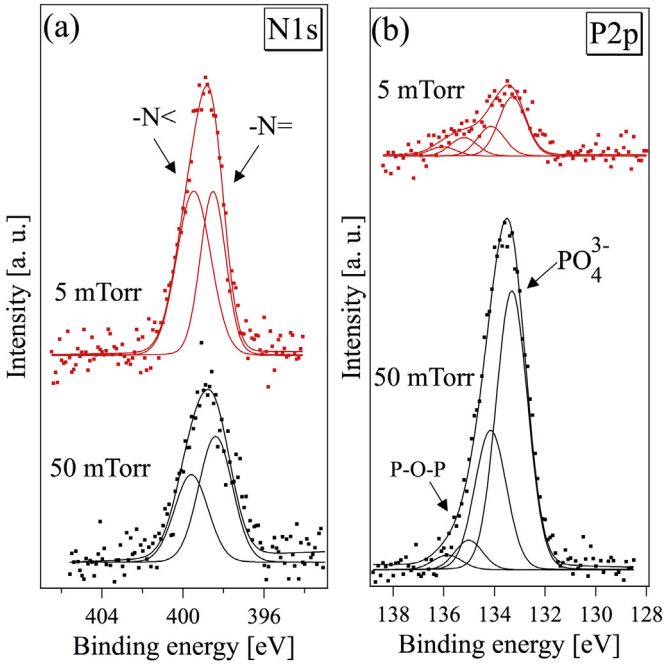

Fig. 14. N1s (a) and P2p (b) peaks by XPS for 5 and 50 mTorr deposited for 100 W in 150 min.

coordinated N bond structure for 5 mTorr while the contribution from the double coordinated bond is higher for 50 mTorr. Some peaks assignment for P2p is included in the figure. A more detailed investigation of the film structure was not approached in this study due to limited capability to handle the samples in a completely controlled atmosphere after the deposition. Park et al. [17] have also investigated the film structure by XPS and found evidence of double and triple coordinated bonds of N for films deposited at 5 and 10 mTorr and no detectable signal for 20 mTorr. The EDS is penetrating the film so the N and P packs can regarded as integration over the whole film thickness for a scanning area of $20 \times 20\ \mu m^2$. The N/P peak ratio was 1.2 for 5 mTorr, 0.97 for 20 mTorr and 0.93 for 50 mTorr, respectively.

3.5. Discussion

As pointed out recently by Muñoz [31] the mechanism controlling the ionic conductivity of Lipon films is not understood and more in-depth studies are necessary as to clarify it. This can also be the result of conflicting data and lack of information coupling the gas phase processes during the transport of sputtered species through plasma with the surface and volume processes responsible for the growth. As no details of the plasma diagnostic has been published earlier, the discussion on the sputtering reaction steps and active species during Lipon deposition, and the effect of sputtering pressure and RF power, has been limited to speculations and assumptions [14,17]. Choi et al. [14] suggested a sputtering process involving $Li_3PO_{4-x}N_x$ species, however, the mass spectroscopy results in this study showed no evidence of any species larger than PN (amu = 45). In addition they suggested that the amount of dissociated nitrogen increases with increasing sputtering power, however, as can be seen in Fig. 8 this is not the case. The N/N_2 ratio actually decreases with sputtering power in the range of 50 W to around 150 W, depending on the nitrogen pressure used. Between 200 W and 300 W the N/N_2 ratio is almost constant.

The effect of nitrogen pressure on the Lipon composition has also been intensely investigated. Park et al. [17] have shown that the content of nitrogen decreases with increasing nitrogen pressure, and using EDS we also observed this trend. As reported by Chiu et al. [41] almost no nitrogen is incorporated into the films when using a nitrogen pressure of 100 mTorr. They relate this to the very low kinetic energy of the sputtered atoms which reduces the ability to break the O–P bonds. Indeed the impinging species are less energetic at higher pressures, a fact confirmed by plasma potential measurements from Fig. 11. At the same time, as is shown in Fig. 8, the content of neutral N_2 species increases with increasing pressure. As suggested by Park et al., these N_2 molecules can adsorb in the growing film and thereby block the access of reactive N^+ species and in turn reduce the nitrogen content in the film. Both effects could thus be possible explanations for the reduced nitrogen content. According to Park et al. [17] the N_2 surface adsorption could also be the explanation of the rough surface structure they obtained at high nitrogen pressure. Whether N_2 adsorption can be used to explain the formation of volcano structures at 50 mTorr observed in this study are not clear, and more detailed investigations are necessary as to confirm such a correlation. One important observation resulting from our measurements is that due to acceleration in the potential difference between V_{pl} and the grounded substrate N^+ can gain more than 9.5 eV at 5 mTorr and 100 W (see Fig. 11) when reaching the substrate. This energy is very close to the dissociation energy of N_2 of 9.79 eV which means that N^+ can induce surface dissociation of N_2 unblocking the N penetration, and even more creating additional reactive N. Besides N^+ accessibility to the surface, another effect must be taken into account, i.e. the nitrogen poisoning of the target. According to Park et al. [17] the content of N^+ in the plasma is constant when using a constant RF power, and thus independent of the nitrogen pressure. However, as can be seen in Fig. 7, this is not the case. The amount of N^+ actually decreases when the nitrogen pressure increases, when keeping the RF power constant at 100 W. It is therefore difficult to neglect the effect of nitrogen target poisoning when changing the nitrogen pressure, as they suggested. An interesting link can be made to the observation by Rho et al. [16], that a lower RF power ($3\ W\ cm^{-2}$ instead of $5\ W\ cm^{-2}$) should be used when using a mixed target of Li_3PO_4 and Li_3N, compared to a standard target of pure Li_3PO_4, in order to obtain maximum nitrogen content and ionic conductivity. This indicates, that the target composition, and thus target poisoning, is an important variable to control in order to describe and optimize the plasma composition.

From XPS measurements it was observed, that the sample prepared at 50 mTorr contains a very large amount of phosphor, primarily in the form of PO_4^{3-}, as compared to the sample prepared at 5 mTorr. From Fig. 3(f) it can be seen, that the structure of the material inside the volcano has a different texture than the corresponding flat Lipon film, possibly due to the formation of a crystalline phase. Unfortunately, no quantitative chemical information could be obtained from the interior of the volcanoes using EDS, as the penetration volume of the high energy electrons in the low-density Lipon structure was too large. Based on the high PO_4^{3-} content a possible explanation could be the formation of γ-Li_3PO_4 as observed by Kim et al. [44] when using a high nitrogen flux. The film grows dominated by surface diffusion (highly dependent on surface composition) which is faster and more important in this case than Fickian diffusion. The film formed at low pressure (5 mTorr) is compact and isotropic and Kirkendall diffusion (that can induce porosity) can mainly take place at the interface with silver and gold layers, which should be a very slow process. Films produced at 50 mTorr show irregular morphology suggesting possible nucleation sites for P. Such film is not usable as electrolyte because it needs to be compact, isotropic, and free of voids or cracks. This suggests that the focus should be on how to increase the conductivity for the good quality films obtained at 5 mTorr. It is widely accepted that magnetron sputtering is less effective in preserving the stoichiometry of the target with respect to pulsed laser deposition or molecular beam epitaxy and this is certainly influenced by the amount of nitrogen assisting the film growth, a step further that also needs to be addressed.

As these examples indicate, the type and composition of reactive species in the plasma are responsible for the chemical composition of the Lipon film. However, in order to get a full, detailed understanding of this, more systematic investigations using a quantitative spectroscopic technique (e.g. X-ray photoelectron spectroscopy) combined with plasma diagnostics and avoiding any air contamination is necessary. This would also help to explain and understand the details of the deposition mechanism. This work only serves as a first attempt to relate the plasma diagnostics to the microstructural and electrochemical properties.

4. Conclusion

In this work detailed plasma diagnostics has been performed during RF sputtering of Lipon and the results have been compared to the microstructure, chemical structure and the electrochemical properties of the deposited thin films. Using plasma diagnostics presents a new approach to better understand how the variation of RF power and nitrogen pressure affects the growth as well as the various properties of the films. Low pressure (5 mTorr) and moderate power (100 W) was found to be most beneficial for the growth of good quality films with a high ionic conductivity. Increasing the RF power (300 W) resulted in a poor film quality due to cracks and

dislocation of large clusters from the target, while increasing the nitrogen pressure (50 mTorr) resulted in a lower deposition rate and a rough microstructure with volcano-shaped structures on the surface. Chemical analysis showed larger nitrogen content in the Lipon layer when using low nitrogen pressure, while a larger content of phosphorous was observed in the surface layer when using a high nitrogen pressure. This could possibly be explained by a P-rich phase inside the volcanoes. Detailed plasma diagnostics showed that the optimal sputter parameters of 5 mTorr and 100 W is correlated with a higher degree of dissociated N_2, lower plasma density, higher electron temperature, higher impinging energy for ions and a larger fraction of Li, P and PN at the substrate. No larger clusters could be detected. As a combination of these plasma properties, high-energetic N^+ species can be accelerated towards the substrate to energies above the N_2 dissociation and improve incorporation of N into the Lipon structure. This could possibly explain the increased nitrogen content at low pressures as well as the improved electrochemical performance.

Acknowledgment

The authors would like to acknowledge Copenhagen Cleantech Cluster for financial support of the project and fruitful discussions with Dr. Johan Hjelm and Dr. Nikos Bonanos.

References

[1] J.B. Bates, N.J. Dudney, G.R. Gruzalski, R.A. Zuhr, A. Choudhury, C.F. Luck, J.D. Robertson, Solid State Ionics 53 (1992) 647–654.
[2] J.B. Bates, N.J. Dudney, G.R. Gruzalski, R.A. Zuhr, A. Choudhury, C.F. Luck, J.D. Robertson, J. Power Sources 43 (1993) 103–110.
[3] A. Patil, V. Patil, D.W. Shin, J.-W. Choi, D.-S. Paik, S.-J. Yoon, Mater. Res. Bull. 43 (2008) 1913–1942.
[4] J.B. Bates, N.J. Dudney, B. Neudecker, A. Ueda, C.D. Evans, Solid State Ionics 135 (2000) 33–45.
[5] I. Seo, S.W. Martin, in: I. Belharouak (Ed.), Solid Electrolytes for Thin-film Lithium Batteries, InTech, Rijeka, 2012, pp. 101–145.
[6] J. Schwenzel, V. Thangadurai, W. Weppner, J. Power Sources 154 (2006) 232–238.
[7] X. Yu, J.B. Bates Jr., G.E. Jellison, F.X. Hart, J. Electrochem. Soc. 144 (1997) 524–532.
[8] L. Le Van-Jodin, F. Ducroquet, F. Sabary, I. Chevalier, Solid State Ionics 253 (2013) 151–156.
[9] M. Koo, K.I. Park, S.H. Lee, M. Suh, D.Y. Jeon, J.W. Choi, K. Kang, K.J. Lee, Nano Lett. 12 (2012) 4810–4816.
[10] S.K. Martha, J. Nanda, Y. Kim, R.R. Unocic, S. Pannala, N.J. Dundey, J. Mat. Chem. A 1 (2013) 5587–5595.
[11] Y. Kim, G.M. Veith, J. Nanda, R.R. Unocic, M.F. Chi, N.J. Dundey, Electrochim. Acta 56 (2011) 6573–6580.
[12] Y. Kim, N.J. Dundey, M.F. Chi, S.K. Martha, J. Nanda, G.M. Veith, C.D. Liang, J. Electrochem. Soc. 160 (2013) A3113–A3125.
[13] N.J. Dudney, J. Power Sources 89 (2000) 176–179.
[14] C.H. Choi, W.I. Cho, B.W. Cho, H.S. Kim, Y.S. Yoon, Y.S. Tak, Electrochem. Solid-State Lett. 5 (2002) A14–A17.
[15] Z. Hu, D. Li, K. Xie, Bull. Mater. Sci. 31 (2008) 681–686.
[16] N.S. Roh, S.D. Lee, H.S. Kwon, Scr. Mater. 42 (1999) 43–49.
[17] H.Y. Park, S.C. Nam, Y.C. Lim, K.G. Choi, K.C. Lee, G.B. Park, S.-R. Lee, H.P. Kim, S.B. Cho, J. Electroceram 17 (2006) 1023–1030.
[18] N. Suzuki, S. Shirai, N. Takahashi, T. Inaba, T. Shiga, Solid State Ionics 191 (2011) 49–54.
[19] Y. Hamon, A. Douard, F. Sabary, C. Marcel, P. Vinatier, B. Pecquenard, A. Levasseur, Solid State Ionics 177 (2006) 257–261.
[20] S. Zhao, Z. Fu, Q. Qin, Thin Solid Films 415 (2002) 108–113.
[21] W.-Y. Liu, Z.-W. Fu, C.-L. Li, Q.-Z. Qin, Electrochem. Solid-State Lett. 7 (2004) J36–J40.
[22] F. Munoz, A. Duran, L. Pascual, L. Montagne, B. Revel, A.C.M. Rodrigues, Solid State Ionics 179 (2008) 574–579.
[23] Y.G. Kim, H.N.G. Wadley, J. Vac. Sci. Technol. A 26 (2008) 174–183.
[24] F. Vereda, N. Clay, A. Gerouki, R.B. Goldner, T. Haas, P. Zerigian, J. Power Sources 89 (2000) 201–205.
[25] C.S. Nimisha, K.Y. Rao, G. Venkatesh, G.M. Rao, N. Munichandraiah, Thin Solid Films 519 (2011) 3401–3406.
[26] B. Fleutot, B. Pecquenard, H. Martinez, M. Letellier, A. Levasseur, Solid State Ionics 186 (2011) 29–36.
[27] S. Jacke, J. Song, L. Dimesso, J. Brotz, D. Becker, W. Jaegermann, J. Power Sources 196 (2011) 6911–6914.
[28] B.J. Neudecker, R.A. Zuhr, J.B. Bates, J. Power Sources 81 (1999) 27–32.
[29] B. Fleutot, B. Pecquenard, H. Martinez, A. Levasseur, Solid State Ionics 206 (2012) 72–77.
[30] B. Wang, B.S. Kwak, B.C. Sales, J.B. Bates, J. Non-Cryst. Solids 183 (1995) 297–306.
[31] F. Muñoz, J. Power Sources 198 (2012) 432.
[32] Bio-logic – Science Instruments, EC-lab Software, V10.32, 2013.
[33] E. Stamate, K. Ohe, Appl. Phys. Lett. 78 (2001) 153–155.
[34] E. Stamate, K. Ohe, J. Vac. Sci. Technol. A 20 (2002) 661–666.
[35] A. Lacoste, T. Lagarde, S. Béchu, Y. Arnal, J. Pelletier, Plasma Sources Sci. Technol. 11 (2002) 407–412.
[36] L. Latrasse, A. Lacoste, J. Sirou, J. Pelletier, Plasma Sources Sci. Technol. 16 (2007) 7–12.
[37] E. Stamate, M. Draghici, J. Appl. Phys. 111 (2012) 083303.
[38] E. Stamate, G. Popa, K. Ohe, Rev. Sci. Instrum. 70 (1999) 58–62.
[39] E. Stamate, K. Inagaki, K. Ohe, G. Popa, J. Phys. D. Appl. Phys. 32 (1999) 671–674.
[40] H. Sugai, H. Toyoda, J. Vac. Sci. Technol. A 10 (1992) 1193–1200.
[41] K.F. Chiu, C.C. Chen, K.M. Lin, C.C. Lo, H.C. Lin, W.H. Ho, C.S. Jiang, J. Vac. Sci. Technol. A 28 (2010) 568–572.
[42] M. Ohring, in: Materials Science of Thin Films: Deposition and Structure, Academic Press, San Diego, 2002, p. 223.
[43] J.A. Thornton, J. Vac. Sci. Technol. A 4 (1986) 3059–3065.
[44] Y.G. Kim, H.N. G Wadley, J. Power Sources 196 (2011) 1371–1377.
[45] J. Chong, L. S. B. Kwak, 2012 WO/2012/174260.
[46] R.F. Egerton, P. Li, M. Malac, Micron 35 (2004) 399–409.